Pergamon

0038-1101(94)00257-6

Solid-State Electronics Vol. 38, No. 7, pp. 1305–1312, 1995

0038-1101/95 $9.50 + 0.00

EVOLUTION OF DISLOCATION LOOPS IN SILICON IN AN INERT AMBIENT—I

J. LIU[1], M. E. LAW[2] and K. S. JONES[1]

[1]Department of Materials Science and Engineering, 214A Rhines Hall and [2]Department of Electrical Engineering, University of Florida, Gainesville, FL 32611, U.S.A.

(Received 18 October 1994)

Abstract—A plan-view TEM study has been made of the distribution, geometry and the time-dependent annealing behavior of type II (end of range) dislocation loops introduced by $1 \times 10^{15}/cm^2$ 50 keV Si^+ implantation into silicon. The size and density distributions of the loops have been quantitatively analyzed, and loop growth behavior has been compared with that predicted by a bulk-diffusion mechanism and by a glide and self-climb mechanism. It has been shown that the loop growth rate is approximately constant for each annealing temperature (700–1000°C) and that the growth is governed by the bulk-diffusion mechanism. Regions of growth and shrinkage have been investigated for different annealing temperatures in terms of interstitial supersaturation and the critical loop growth radius. The activation energy for loop growth is determined to be 1.0 ± 0.2 eV from the Arrhenius plot of loop growth rate versus the reciprocal of annealing temperature.

1. INTRODUCTION

It is well known that post-implantation annealing of silicon can result in the formation of dislocation loops[1]. These loops can in turn affect dopant diffusion through the gettering of dopant and the trapping and release of excess point defects. Thus, knowledge of the annealing kinetics of dislocation loops and their effect on point defects is essential for accurate silicon integrated circuit processing modeling. However, to date no complete studies of the loop growth, coarsening and dissolution phases have been reported for inert ambient annealing conditions. This work studied the loop evolution process without an external source of additional defects, and therefore provides a basis for understanding the interaction between processing-induced dislocation loops and point defects which further is essential to modeling dopant diffusion.

Basically two mechanisms have been proposed for the growth of dislocation loops during thermal annealing[2,3]. The first is based on bulk diffusion-controlled climb. The second is the aggregation and coalescence of loops as a result of glide and self-climb. According to the bulk diffusion mechanism, dislocation loops grow or shrink through the diffusion of point defects between the loops and the driving force for the process is provided by the self-energy of the dislocation loops. On the other hand, the glide and self-climb mechanism regards the elastic interaction between two nearby loops as the driving force tending to create a short-circuit diffusion around the periphery of the loops. This accounts for the coalescence of coplanar loops, which is the self-climb process. Loops can also move along a cylindrical surface containing the Burgers vector and this is the so-called glide process. Since the loops studied in this investigation are extrinsic and prismatic in character, they grow by either the diffusion of interstitial atoms to the loops or by the diffusion of vacancies from the loops[4–9].

As early as 1960, Silox and Whelan[10] and Vandervoort and Washburn[11] observed that the density of loops present in as-quenched aluminum decreased markedly upon annealing. Silox and Whelan have accounted for these observations by proposing that vacancies are evaporated from the periphery of each loop and these vacancies then diffuse to the surface of the foil. In the same year, Johnson[2] proposed that the coalescence of quenched-in dislocation loops in aluminum took place by short-circuit diffusion around the periphery of each loop. In 1971, electron transmission microscope studies were made of the annealing behavior of defect clusters in neutron-irradiated molybdenum by Eyre and Maher[3]. They found that the interstitial loop growth observed in molybdenum neutron-irradiated at 77 K was accounted for by a glide and self-climb mechanism. On the other hand, the vacancy loop growth observed in molybdenum neutron-irradiated at 473 K could be accounted for by a bulk vacancy diffusion mechanism, although both mechanisms contributed to the growth at intermediate stages of the anneal. Despite numerous studies of implantation induced dislocation loops, this work attempts to understand the time-dependent annealing behavior of Si self-implantation induced Si interstitial loops and to find out the mechanism by which loops evolve during the anneal.

2. EXPERIMENTAL

The starting materials used in this experiment were Czochralski single crystal wafers of (100) orientation. The boron doped p-type wafers were of resistivity $1 \sim 100\ \Omega$cm with thickness of $600 \sim 650\ \mu$m. Type II dislocation loops were formed from ion implantation damage produced via implantation of Si^+ into Si at 50 keV and a dose of $1 \times 10^{15}/cm^2$. The implant temperature was kept around room temperature and was stabilized during the implantation using a Way-flow Freon cooled endstation. The dose rate was $20\ \mu A/cm^2$ and was kept constant during the implant process. These conditions resulted in the formation of a continuous amorphous layer. The type II or EOR (end of range) loops formed upon annealing just below the amorphous/crystalline interface about 1200 Å deep, as determined by cross-sectional TEM measurements.

After implantation, the whole wafer was capped with 6000 Å SiO_2 before the annealing process to limit oxidation in inert ambient. Then the wafer was cut into four parts and subjected to annealing in nitrogen at 700, 800, 900 and 1000°C respectively, for times of 15 min, 30 min, 1 h, 2 h, 4 h and 16 h at each temperature. The capped oxide for all 24 samples was removed by HF before mechanical lapping of the back side and jet etching to form the plan-view samples. Plan-view transmission electron microscopy (PTEM) samples were made using a South Bay Technology (Model 550C) jet etcher and an $HF:NHO_3 = 1:3$ solution.

By counting loop numbers and measuring loop size (area) with PTEM on a JEOL 200CX TEM, it was possible to determine quantitatively the concentration of interstitials trapped by the type II dislocation loops[12]. The analysis was performed using weak-beam dark field (g_{220}) images of annealed PTEM samples. By assuming a circular loop, the radius of each loop or partial loop was measured along its longest axis and the corresponding loop area was calculated. The average loop radius was calculated by choosing radius intervals of 35 Å for 700–900°C and 50 Å for 1000°C, assuming loops all have the same radius in each interval, counting the number of the loops and averaging the radius values within the whole range. The average radius can also be deduced from the stack histogram of the radius distribution by fitting with a gaussian function[13], but this was not used in our study. The concentration of atoms bound by the loops could be estimated by multiplying the fraction of loop area by the atomic density of atoms on the {111} plane, which is $1.6 \times 10^{15}/cm^2$. By these methods we can determine the concentration of dislocation loops, the concentration of interstitials bound by the loops, the loop distribution and loop growth rate for different annealing times at each annealing temperature. Furthermore, by comparing the loop growing rates with the rates predicted by the bulk-diffusion and glide and self-climb theories, we can decide which mechanism best accounts for the loop growing behavior.

3. RESULTS AND DISCUSSIONS

The weak-beam dark field g_{220} PTEM micrographs are shown in Fig. 1(a), (b), (c) and (d), after annealing at temperatures of 700, 800, 900 and 1000°C respectively. It is apparent that as the annealing temperature increases, the average size of the loops increases. If the temperature is kept constant, the loop size increases with increasing annealing time, although at lower temperatures (700, 800°C) this growth appears to be much slower than that at high temperatures (900, 1000°C). In the mean time, the total loop density is decreasing which makes the density of interstitial bound by the loops stay constant for low temperature annealing and decrease after annealing at high temperatures (i.e., $\geqslant$900°C). For annealing times greater than 2 h at 1000°C, very few loops remain and they evolve into stacking faults.

The loop radius was measured for each annealing condition and the average value $r_{avg} = \Sigma N(r)r/N_L$ was calculated by adding the product of the loop radius r and the fraction of loops with that radius $N(r)/N_L$, where N_L is the total loop density. Figure 2 shows the average loop radius versus annealing time at different temperatures. As we can see, the general tendency is that the loop radius increases along with the annealing time, although it is very slow at low temperatures. At the early stage of 700°C annealing, the loops are quite small, but after 4 h annealing, they are well developed.

The total loop densities versus annealing time at different temperatures are shown in Fig. 3, where we can see that the loop density decreases with time, and if the time is kept constant, it decreases as the temperature increases. This is the result of the loop coarsening process, during which the larger loops grow at the expense of smaller ones. At higher annealing temperatures the interstitials diffuse to the surface or into the bulk resulting in an insufficient concentration to stabilize even the larger loops. When this occurs, the loops enter the dissolution regime. After 1000°C annealing, the loop density is seen to decrease rapidly. Figure 4 shows the density of interstitials bound by the loops as a function of annealing time. For 700 and 800°C annealing, the loops remain in the coarsening regime and the density of the interstitials bound by the loops is constant during the annealing process. For 900°C annealing, after 30 min the interstitial density decreases and the loops change from the coarsening regime to the dissolution regime. After only 15 min annealing at 1000°C, the loop dissolution process starts and the interstitial density reaches a very small value ($\leqslant 3 \times 10^{12}/cm^2$) after 2 h. Unfortunately, oxidation occurs after that and stacking faults form before complete loop dissolution. It is also apparent from Figs 2 and 4 that when temperature increases, after

for example 15 min anneal, the average loop radius increases, which means more of the implantation induced interstitials move into the dislocation loops. The evolution of the size distribution $N(r)$ versus radius r was also measured. These results and the modeling of these results are presented in Part II of these papers.

As we pointed out before, two possible models to explain the loop growth are either the bulk diffusion mechanism or the glide and self-climb mechanism. A main distinction between these two mechanisms is that they predict different loop growth rate dependencies on time. According to bulk diffusion mechanism, the radii of growing loops are proportional to t, where t is the annealing time. This implies a uniformly increasing average loop radii. According to the glide and self-climb mechanism, the radii of growing loops are proportional to $t^{2/13}$. This implies a rapid initial increase in average loop radii, followed by much smaller increases[3]. To distinguish between these mechanisms, a plot (Fig. 5) of the growth rate of the loops versus time along with values predicted by both mechanisms has been made. The experimental data are plotted in scattered points. The results indicated that the loop growth rates remain almost constant during coarsening and dissolution processes, in other words, the average loop radii increase approximately linearly with time. In addition, the loop growth rates increase with the increase of annealing temperature.

The horizontal full lines in Fig. 5 correspond to bulk diffusion mechanism predictions, while the inclined dotted lines correspond to the glide and self-climb mechanism predictions. The lines which have larger y-intercepts are the cases for higher annealing temperatures. The plots are made in logarithmic scales on both axes since the $t^{2/13}$ dependence of growth rate in glide and self-climb mechanism will be shown as straight lines in log–log plots with a slope of $-11/13$. As we can see, the experimental data fall

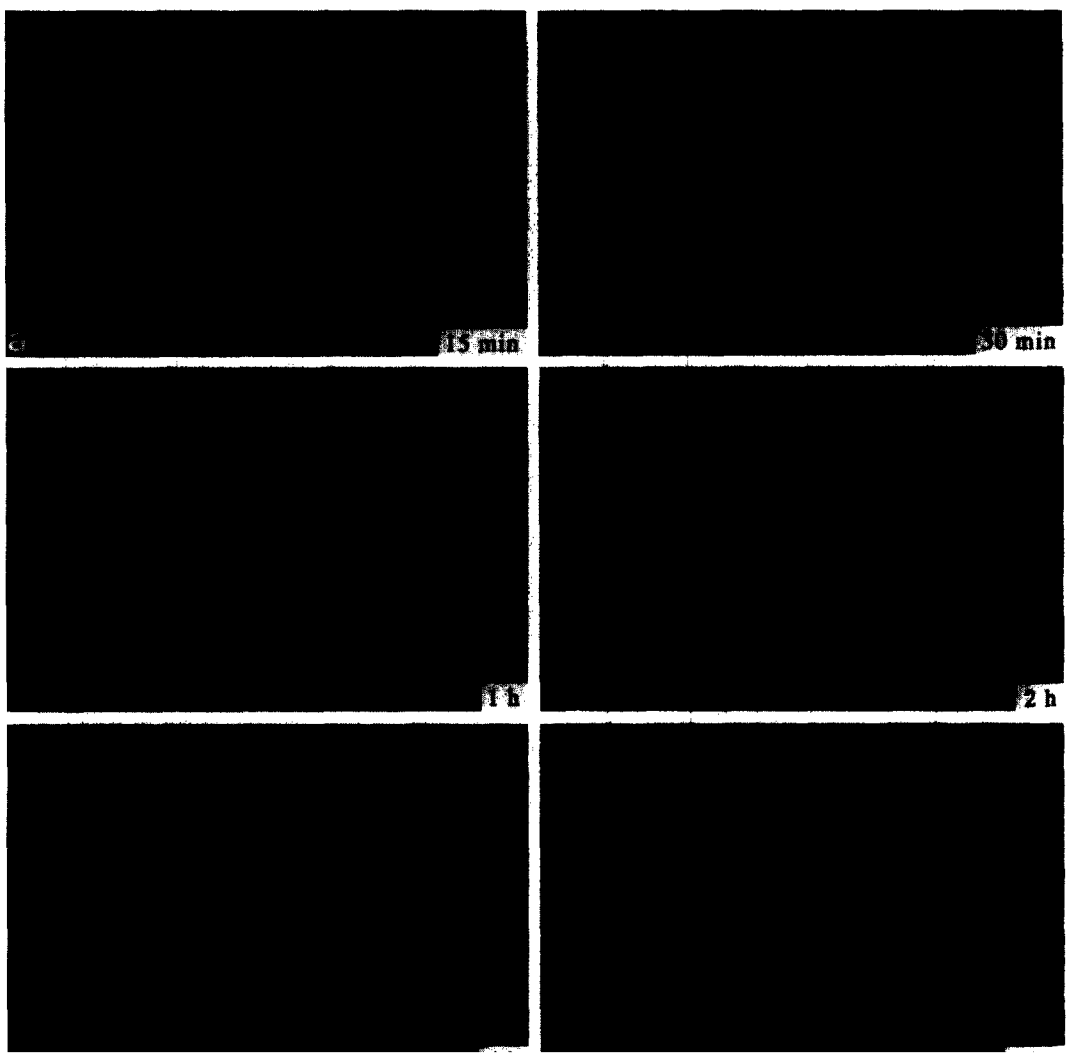

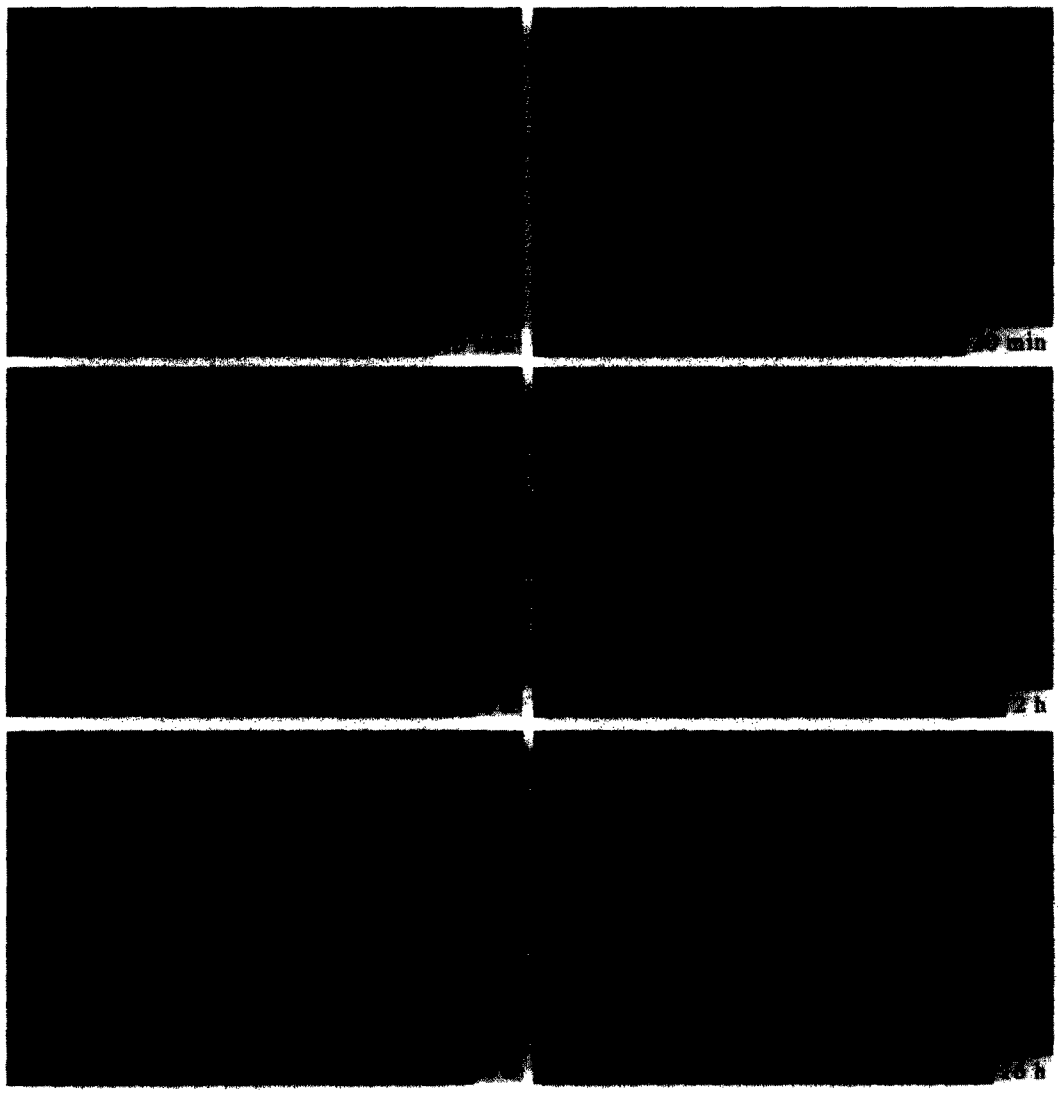

Fig. 1(b)—*Caption on page 1310*

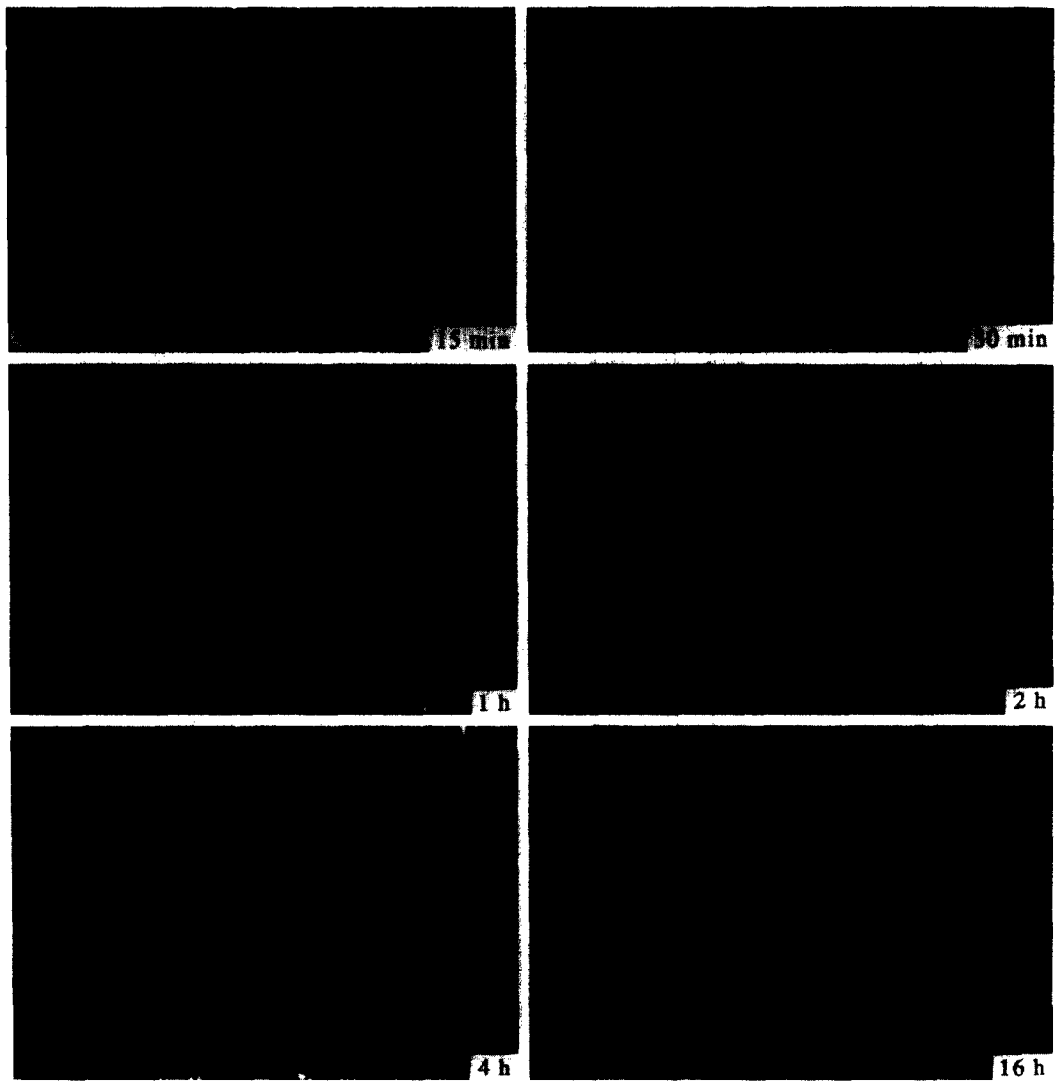

Fig. 1(c)—*Caption overleaf*

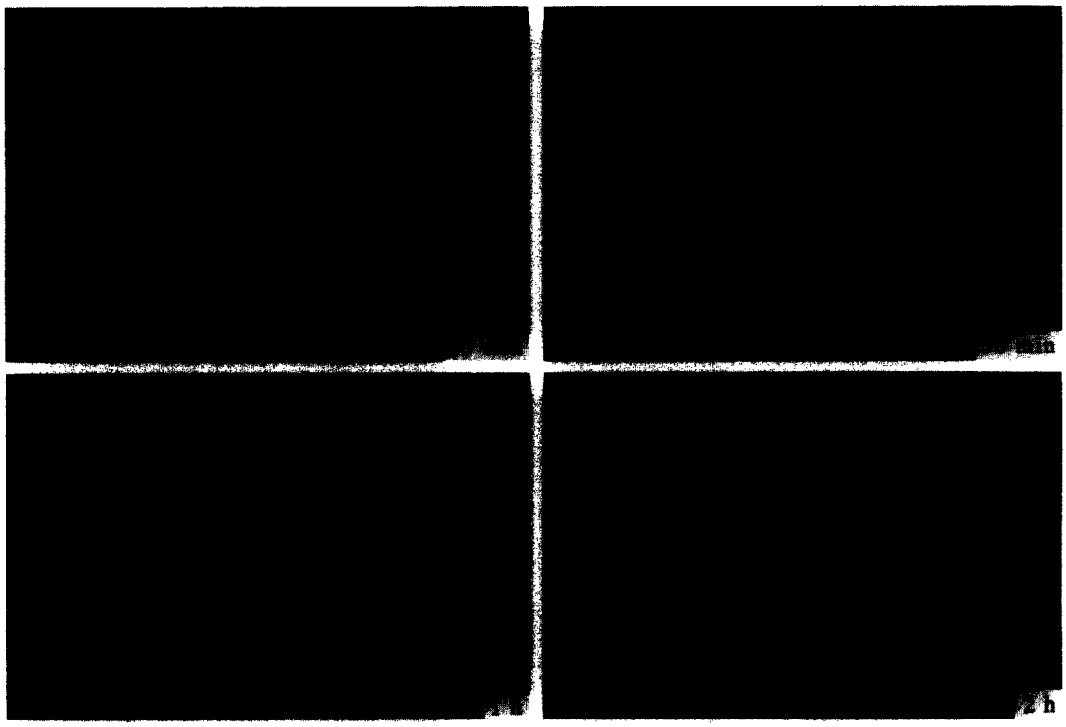

Fig. 1(d).

Fig. 1. Weak-beam dark field g_{220} PTEM micrographs for various annealing conditions.

almost exclusively on the bulk diffusion predicted lines so we conclude that the mechanism governing the loop growth in our experiment in bulk diffusion. The simulated values of average loop radius versus annealing time using bulk diffusion mechanism are presented in Fig. 2 together with the experimental values. The average loop radius is the only variable that can be modeled by this simple method. In order to model the subtle changes in the size distribution, a more complete model is necessary as discussed in Part II of these papers.

It is possible to determine the activation energy for loop growth by producing an Arrhenius plot ($v = v_0 \exp(-E/kT)$) of the average velocity of loop growth versus the annealing temperature, as shown in Fig. 6. The activation energy E has been found to be 1.0 ± 0.2 eV, which reflects a complex process, including the shrinkage of the small loops and the migration of interstitials from smaller loops to the large.

A rate theory model for interstitial dislocation loop growth by bulk-diffusion was proposed by Eyre and Maher[3]. When the bulk diffusion mechanism is

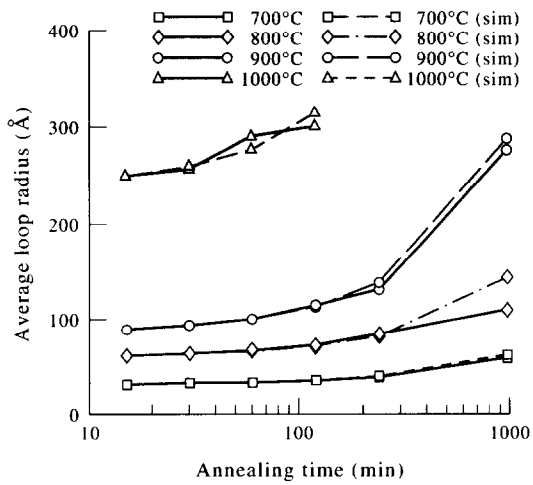

Fig. 2. Experimental and simulated average loop radius as a function of annealing time at different temperatures.

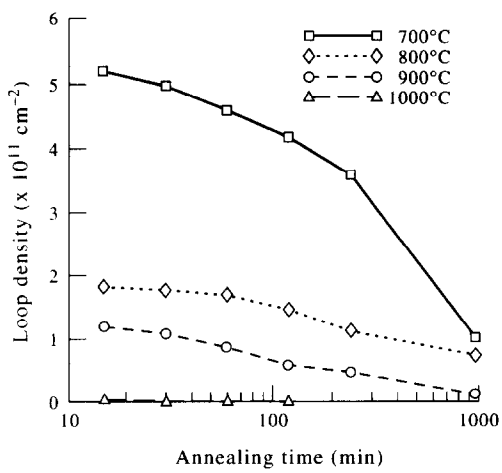

Fig. 3. Variation in total loop density as a function of annealing time at different temperatures.

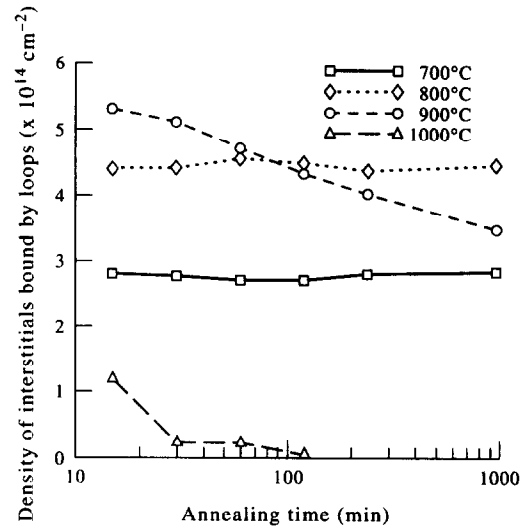

Fig. 4. Variation in density of interstitials bound by dislocation loops as a function of annealing time at different temperatures.

operative, loop growth or shrinkage occurs by diffusion of point defects to from the loops via the matrix. Assuming diffusion controlled growth and shrinkage will occur by an interstitial mechanism, the concentration gradient of self-interstitials among loops induces a flux from smaller loops to larger ones (the interstitial concentration around larger loops is lower than that around smaller loops). As a result, larger loops grow and smaller loops shrink until they eventually dissolve. Emission or adsorption of an interstitial by a perfect loop results in a change in its elastic energy $\Delta E_S = \tau \mathbf{b}^2 r$, where τ is the line energy given by:

$$\tau = \frac{\mu \mathbf{b}^2}{4(1-\nu)} \ln \frac{4r}{\mathbf{b}}. \tag{1}$$

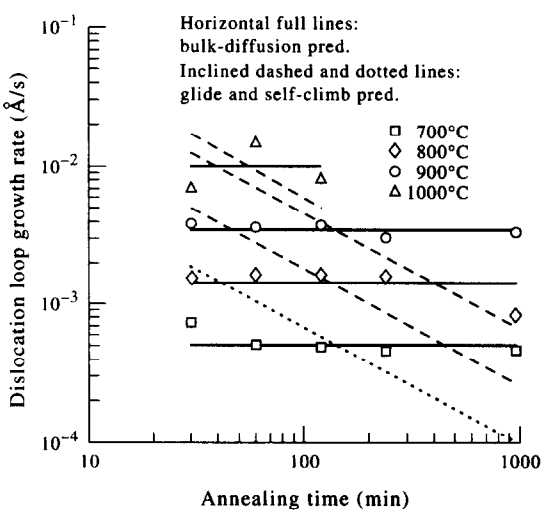

Fig. 5. Experimental and predicted loop growth rate versus annealing time at different temperatures. The horizontal full lines correspond to bulk-diffusion mechanism prediction and the inclined dotted lines correspond to glide and self-climb mechanism prediction.

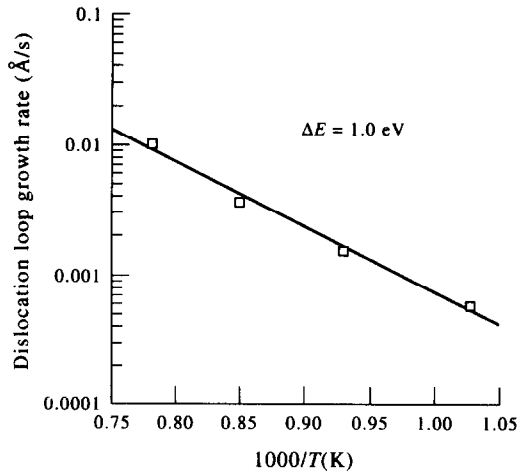

Fig. 6. Loop growth rate versus $1000/T$.

Here, μ is the shear modulus, ν is the Poisson's ratio, $\mathbf{b}$ is the Burgers vector. In the case of interstitial loops, at any annealing temperature T, there is a concentration of interstitials in local equilibrium with interstitial loops given by:

$$C_L = C_0 \exp(\Delta E_s / kT) = C_0 \exp(\tau \mathbf{b}^2 / rkT), \tag{2}$$

where C_L is the interstitial concentration around the loops, C_0 is the thermal equilibrium concentration of interstitials in the bulk crystal and k is the Boltzmann's constant. The rate equation describing the growth and shrinkage of interstitial dislocation loops is obtained as:

$$\frac{dr}{dt} = AD\left[\frac{C}{C_0} - \frac{C_L}{C_0}\right] = AD\left[\frac{C}{C_0} - \exp\left(\frac{\tau \mathbf{b}^2}{rkT}\right)\right], \tag{3}$$

where D is the self-diffusion coefficient and C is the interstitial concentration between the loops. Constant A is a geometrical factor depending on the boundary conditions for diffusion and takes the form $A = 4\sqrt{3}/\pi a$, where a is the interatomic distance. An important practical consequence of eqn (3) is that an essential condition for growth of an interstitial loop is an interstitial supersaturation in the surrounding crystal. If C/C_0 is greater than C_L/C_0, interstitials will be transported to the loop and loop growth occurs. On the other hand, if C/C_0 is less than C_L/C_0, interstitials will be moved away from the loop and loop shrinkage occurs. Moreover, it follows that for any given values of $C/C_0 \neq 1$, a critical radius, r_{crit}, can be defined as:

$$r_{crit} = \frac{\tau \mathbf{b}^2}{kT \ln \dfrac{C}{C_0}}, \tag{4}$$

such that when $r > r_{crit}$, dislocation loop growth occurs and when $r < r_{crit}$, loop shrinkage occurs.

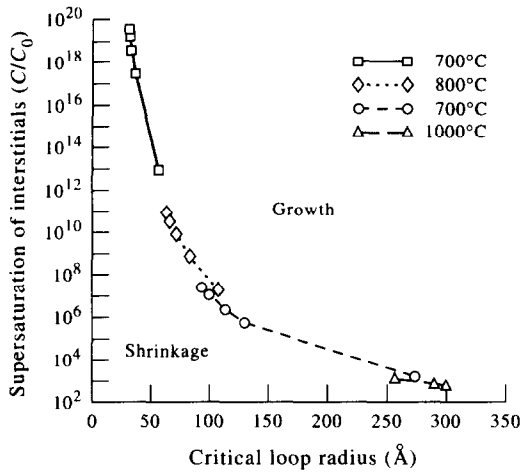

Fig. 7. Supersaturation of interstitials during annealing versus critical loop radius.

Consider now the diffusion-limited growth and shrinkage of a random loop distribution, $N_{(r)}$, predominantly of one defect type and where $N(r)\,dr$ is the number of loops having radii lying between r and $r + dr$. Clearly an increase in the average loop radius $r_{avg} = \Sigma N(r)r/N_L$ requires a redistribution in the loop population such that large loops grow at the expense of small ones.

Substituting the values of loop growth rates at different loop radii into eqn (3), we can find values of C/C_0, and furthermore, by substituting values of C/C_0 into eqn (4), we can find out the critical radii r_{crit} for loop growth. In carrying out the calculations, values appropriate to silicon at room temperature, which are believed to be good approximations at the annealing temperatures, have been used for the material constants and these are $a = 2.7$ Å, $\nu = 0.27$, $\mu = 7.55 \times 10^{11}$ dyn/cm^2. The critical loop radius, r_{crit}, defining the boundary between growth and shrinkage of loops, has been plotted as a function of C/C_0 in Fig. 7, where regions corresponding to loop growth and shrinkage at each temperature are indicated. As can be seen, values of C/C_0 are decreasing with annealing time, which means the interstitial supersaturation is a strong function of loop radius. For higher temperature annealing, since the diffusivity of interstitials is much larger, the loop sizes reach larger values more quickly.

4. CONCLUSION

The loop coarsening and dissolution features have been exposed by the results of the time-dependent post-implantation annealing behavior. It is shown that the loop density goes down whereas the loops grow in size during the annealing. The interstitials bound by the loops keep constant during the coarsening process and decrease during the dissolution process. By considering the relevance of the experimental observations and the predictions of two loop growth mechanisms, the changes in size of the interstitial loops introduced by implantation can be satisfactorily accounted for by a bulk diffusion mechanism, not the glide and self-climb mechanism. The activation energy for the loop growth has been found to be 1.0 ± 0.2 eV.

Acknowledgements—The authors are grateful to Drs Viswanath Krishnamoorthy and Jian Chen for their stimulating discussions, and Dr. David Eaglesham for his insight into the activation energy calculation. The authors would also like to thank SEMATECH and IBM for supporting this work.

REFERENCES

1. K. S. Jones, S. Prussin and E. R. Weber, *Appl. Phys. A* **45,** 1 (1988).
2. C. A. Johnson, *Phil. Mag.* **5,** 1255 (1960).
3. B. L. Eyre and D. M. Maher, *Phil. Mag.* **24,** 767 (1971).
4. R. B. Fair, J. J. Wortman and J. Liu, *J. electrochem. Soc.* **131,** 2387 (1984).
5. M. Servidori, Z. Sourek and S. Solmi, *J. appl. Phys.* **62,** 1723 (1987).
6. K. S. Jones, S. Prussin and E. R. Weber, *J. appl. Phys.* **62,** 4114 (1987).
7. T. O. Sedgwick, A. E. Michel, V. R. Deline, S. A. Cohen and J. B. Lasky, *J. appl. Phys.* **63,** 1452 (1988).
8. Y. Kim, H. Z. Massoud and R. B. Fair, *J. Electron. Mater.* **18,** 143 (1989).
9. Y. M. Kim, G. O. Lo, H. Kinoshita, D. L. Kwong, H. H. Tseng and R. Hance, *J. electrochem. Soc.* **138,** 1122 (1991).
10. J. Silox and M. J. Whelan, *Phil. Mag.* **5,** 1 (1960).
11. R. Vandervoort and J. Washburn, *Phil. Mag.* **5,** 24 (1960).
12. K. S. Jones and D. Venables, *J. appl. Phys.* **69,** 2931 (1991).
13. L. Laânab, C. Bergaud, C. Bonafos, A. Martinez and A. Claverie, *IIT Meeting Proc.*, Italy (1994).